Towards the use of Integral Radar Volume Descriptors for quantitative areal precipitation estimation - results from pseudo-radar observations

Silke Trömel*, Clemens Simmer

Meteorological Institute of the University Bonn, Germany

Jürgen Braun, Thomas Gerstner, Michael Griebel

Institute for Numerical Simulation of the University Bonn, Germany

* *Corresponding author address:* Silke Trömel, Meteorological Institute of the University Bonn, Germany.

E-mail: silke.troemel@uni-bonn.de

ABSTRACT

The central objective of our analysis is to significantly enhance the quality of radar derived precipitation estimates by as fully as possible exploiting the information contained in the spatial and temporal variability of 3D radar volume data. The results presented are yet based on pseudo-radar data and rain rates of a regional weather forecasting model and 12 true radiosoundings as well. We pursue two approaches: The first approach estimates total rainfall from an individual storm over its lifetime while the second approach assesses the areawide instantaneous rainfall from a multiplicity of such storms by the use of measurements of the areal coverage of the storms exceeding a threshold radar reflectivity. We extend the concept by adding further predictors in order to significantly enhance the rainfall estimates. The horizontal expected value and the horizontal standard deviation of enclosed reflectivities at the ground, the mean brightband fraction and its trend, the fractional area with reflectivities exceeding a threshold τ and an orographic rainfall amplifier provide relative errors smaller than 10% in approximately 75% of the considered rain events in the first approach. In the second approach we achieve a relative error below 10% in approximately 63% elements of the test set.

1. Introduction

Flash flood forecasting, the engineering design of flood control structures, and the operation and control of sewerage systems or water supply forecasting require quantitative areal precipitation estimates which challenge the potential of current observation systems (Krajewski and Smith, 2002). The range of temporal and spatial scales involved in precipitation generation especially in convective situations renders current rain gauge networks largely inappropriate for this task. The existing ground based radar networks have by far the largest potential to provide adequate space-time distributions of surface rainfall for any hydrological and also meteorological application.

Radar-derived precipitation estimation is, however, still hampered by a range of error sources. Besides ground clutter, beam blocking, anomalous propagation and attenuation the uncertainty of the so-called Z-R-relations – the transformation of the measured radar reflectivity Z into an estimate of the local precipitation intensity R – alone can cause errors up to 200% (Fabry et al., 1992). Despite intensive research since the dawn of radar meteorology, one of the first Z-R-relations ever published – the famous relation by Marshall et al. (1955) – is still most frequently used for the operational conversion of radar reflectivities into rain rates. Dynamic Z-R-relations, which follow the changes in the drop size distributions caused by changing regimes in the precipitation generation process might be the best solution in the end, but we still miss both, the knowledge of an exploitable connection between these regimes and related dropsize distributions as well as a method to detect these regimes from available observations. The exploitation of polarization has up to now mainly led to a much better identification of different hydrometeor types and a reduction of attenuation effects. Even

though promising approaches in quantitative rainfall estimation with polarimetric radar exist (Ryzhkov et al., 2005), they have not yet materialized in operational applications.

In this paper, we introduce two approaches which completely abandon the concept of local precipitation intensity estimation by Z-R-relations, which in our view has hindered quantitative precipitation estimation by a too narrow interpretation of the radar data. We hypothesize that an improved quantitative areal precipitation estimation can be achieved by more extensively exploiting the spatial and temporal variability of the radar signals produced by the complete precipitation generating system, e.g., by a convective cell during its life span. We have to concede that this concept will not provide immediate access to the local instantaneous rain rates requested, e.g., by hydrology; but we might be able to provide more reliable estimates of rainfall integrated over time or space, which in turn can be used to constrain estimates based on local Z-R-relations using a disaggregation technique (Hagen et al, 2003).

We search for so-called Integral Radar Volume Descriptors (IRVD), which can be derived from the three dimensional radar volume data and which are supposed to contain relevant information on the underlying precipitation process. This idea is not new; Doneaud et al. (1981) investigated a technique for estimating the total rain volume of precipitation events from radar data without invoking a Z-R-relationship. They found that the total rainfall produced by individual storms can also be estimated simply by considering only the horizontal extent and the duration of radar-observed precipitation. Doneaud et al. (1981) however, did not present a convincing explanation for the high correlations found. Later, Atlas et al. (1990) recovered their approach and presented a unified theory for both, the estimation of the total rainfall of an individual storm and for the average instantaneous rain

rate from a multiplicity of such storms. Our re-analysis of their theory and extension of their concept with IRVDs is not yet based on real radar data but on pseudo-radar data derived from simulations with a regional weather forecasting model. On one hand, this will limit the conclusions from the study to a demonstration of the potential of the method (without proving it in the real world). Assuming that current atmospheric models sufficiently describe the dynamics and microphysics of precipitation processes, the study will, however, give an upper limit to accuracies achievable with real radar data. On the other hand, current direct precipitation measurement networks consisting of rain gauges alone are insufficient for a validation and further exploitation of the concept. We will discuss ways to circumvent this problem later in the paper.

The outline of this paper is as follows. Section 2 summarizes the main concept of the unified theory by Atlas et al. (1990). After describing the data base for our analysis in Section 3, we will introduce an enhancement of the method by defining a suite of integral radar volume descriptors (IRVD) in Section 4. Section 5 shortly introduces the regression methods, and results of their application including the new IRVDs are presented in Sections a and b. Finally, conclusions and an outlook are given.

2. Basics

Atlas et al. (1990) developed a unified theory for the estimation of both,

1. the total rainfall produced by an individual convective storm over its lifetime, and

2. the areawide instantaneous rainfall from a variety of such storms

from the measurements of the areal coverage of storms above a threshold radar reflectivity.

In the first case, the volume rainfall V, defined as the integral of the instantaneous local rain rate R both, over the entire area A_o and over the storm duration T, is estimated by the product of the so-called area-time integral (ATI) of the radar echo in excess of a specified threshold τ over the lifetime of the storm with a factor $S(\tau)$:

$$V = S(\tau) \cdot ATI. \tag{1}$$

ATI is approximated by the sum of the areas a_i with reflectivities above τ over the time intervals Δt_i:

$$ATI \approx \sum a_i \Delta t_i \tag{2}$$

In the second case, the average areawide rain rate $\langle R \rangle$ is estimated from the fraction of the area $A(\tau)$ with reflectivities above the threshold τ divided by the overall considered area A_0:

$$\langle R \rangle = S(\tau) \frac{A(\tau)}{A_o}. \tag{3}$$

The common coefficient $S(\tau)$ in both equations depends on the population distribution of the rain rate R via

$$S(\tau) = \frac{\int_0^\infty RP(R)dR}{\int_\tau^\infty P(R)dR}, \tag{4}$$

where P(R) denotes the value of the probability density function (pdf) at the rain rate R. The approaches of Doneaud et al. (1981) and Atlas et al. (1990) obviously assume that $S(\tau)$ is constant for a given threshold τ, i.e. the theory relies on the existence of a well-behaved pdf of the rain rate either of a single storm during its lifetime, or of an ensemble of storms during one time instant. A storm undergoes typical changes in its appearance during its lifetime, e.g. the growing stage, the convective and the stratiform stage. A well-behaved pdf thus

means that all storms follow similar sequences of stages producing similar rain rates during their lifetimes. Deviations between the resulting pdfs of the storms are thus responsible for the scatter of V about a regression line between V and ATI. Doneaud et al (1981) and Atlas et al. (1990) assume that this scatter is small and a climatological distribution of R can be used. Analogously, a multiplicity of different cells in different stages of evolution in the observational area are sufficient for the existence of such a well-behaved pdf in the second case.

3. Data base: pseudo-radar data and modelled precipitation

Ground-based radars measure the temporally and spatially distributed backscattering of microwave radiation by precipitation-size hydrometeors. More precisely, the backscattered microwave radiation depends on the size, shape and phase of the hydrometeors as well as on their density within the radar volume. The quantitative development of the IRVD method, needs a sufficiently dense station network of rain gauges providing temporally highly-resolved measurements to estimate areal precipitation in the first place. Our first attempts with radar data led to the conclusion that even the existing German network of gauges with higher than daily resolution does by no means satisfy these conditions, i.e. many storms pass the network mostly undetected. Moreover, real radar data suffer from the various errors mentioned above. To circumvent these problems in a first evaluation of the methodology, we have chosen to base our analysis on pseudo-radar data and modelled precipitation, which can

be easily obtained from runs of a meso-scale weather prediction model. We used simulations of the operational Lokal-Modell of the German Weather Service (DWD), which became recently the regional forecast model COSMO of the European Consortium for Modelling (see http://www.cosmo-model.org). The general goal of COSMO is to develop, improve and maintain the non-hydrostatic limited-area atmospheric model, which is used for both for operational and for research applications by the members of the consortium. The national meteorological services of Germany, Switzerland, Italy, Greece, Poland and Romania are COSMO members. In the analysis we use the pseudo-radar data and rain rates generated by COSMO-DE (version LM3.16), a 2.8 km resolution version of COSMO (Doms et al., 2002, 2005) centered over Germany for a period of three days: July 17, 2004, July 8, 2005 and August 19, 2005. The data used is available in 0.025 degree spatial (roughly 2.8 km) and 10 minutes temporal resolution. Figure 1 shows one snapshot of the pseudo-reflectivities at the bottom layer for each day considered, respectively. On July 17, 2004, a convergence line with strong thunderstorms traverses the model area in a northeastern direction. On the second day considered, on July 8, 2005, a multiplicity of cells were rotating about a low-pressure area centered over central Europe. From August 19 to 23 a weather system prevailed in Central Europe, which often results in prolonged and heavy precipitation. In these cases a low pressure front develops in the Gulf of Genoa. This front moves warm, moist air in a north or north-easterly direction until it hits the Alps where it is forced upwards. We included August 19, 2005 in our analyses.

In COSMO-DE grid-scale clouds and precipitation are described using single-moment bulk schemes, i.e. Kessler type (Kessler, 1969). The non-precipitation water categories are supposed to be monodisperse whereas the precipitation particles (rain, snow, graupel)

are assumed to be exponentially distributed. For raindrops this distribution is called the Marshall-Palmer distribution (Marshall and Palmer, 1948). The pseudo-radar reflectivities for these precipitation particles are calculated assuming Rayleigh scattering (Sauvageot, 1992) under the assumptions of the single-moment bulk scheme. It is worth mentioning that graupel and snow particles are calculated as wet particles above 0^oC, i.e. the particles receive a water-coat. Consequently, the so-called brightband can be detected in the pseudo-radar data. Cloud ice and cloud water are neglected in the reflectivities. Altogether, the reader should keep in mind, that the variability of the droplet and particle size distribution is only partially taken into account.

In order to pursue the first approach (total rainfall estimation of a single storm) the SARTrE (Scale Adaptive Radar Tracking Environment)-tracking algorithm (Simon, 2004) is applied to the field of reflectivities near the ground (bottom layer). An edge detection operator strategy is performed including prior smoothing and subsequent application of the Mexican hat operator, an established approach in digital image processing. The successive application of the Gaussian kernel smooths the reflectivity field into coarser and coarser structures with increasing standard deviation of the kernel, thus providing the opportunity to focus the analysis on different scales. One hundred rain events with time spans between 1 and 10.5 hours could be traced. These pursued rain events can consist of several cells, of one single continuous cell or a raining system at large but convective systems dominated at the 3 days considered. The accumulated enclosed area of the traced systems ranges between $0.36 \cdot 10^4\,\mathrm{km}^2$ and $174.287 \cdot 10^4\,\mathrm{km}^2$. In Table 1, the number of observed storms and the standard deviation σ of the applied Gaussian kernel are listed for the three days. Using $\sigma = 6$ results in 141 different cells on July 8, 2005, in the time step shown in Figure 1

(middle) for example.

The computation of the stationary quantities in (3) needed for the second approach does not require the application of the costly SARTrE-tracking algorithm. All values can be directly derived from the COSMO-DE output: To compute the IRVDs we randomly sample for $\tau = 18\,\mathrm{dBZ}$, areas of arbitrary size A_o while the fraction $A(\tau)/A_o$ – the area with reflectivity above a threshold τ and the total area – has to be larger than a predefined threshold F_0. We investigate three different choices of the value, i.e. we take $F_0 \in \{0, 0.01, 0.05\}$. Concerning $\tau = 18\,\mathrm{dBZ}$ we follow Lopez et al. (1983). They used radar data from the Florida Area Cumulus Experiment (FACE), integrated areas in excess of this threshold and found high correlations between daily rainfall volumes and time-averaged areal coverage. The restriction $A(\tau)/A_o \geq F_0$ is motivated by a verification of (3) on the data (see below). Randomization is done in the following way: First, the complete rectangular area of the model domain is split into four rectangular subdomains of the same size and one is randomly chosen. Then, the location of the global maximum of $\langle R \rangle$ in the subdomain is determined which is also a local maximum of the whole area. Finally, two points are sampled randomly from the full domain assuming a Gaussian distribution with $\sigma = 0.3$ unit edge length of the observation area and expected value at the, previously computed, local maximum. The two points then define a rectangular area of size A_o and we test if $A(\tau)/A_o \geq F_0$. If this is not the case then the field is discarded. This procedure is applied separately for each time step for the pseudo-radar data from the three days. As well as in the first approach, the area addressed in this approach may contain several raining systems in large and convective cells. The areas A_o that are selected by this method range from a size of $7.73\,\mathrm{km}^2$ to $9.53 \cdot 10^5\,\mathrm{km}^2$ and for each area the IRVDs, that will be defined in the following, can be directly computed.

For both approaches, the knowledge of temperature and pressure in different heights is needed for the calculation of some IRVDs defined in Section 4. These variables are, however, not taken from the model output but are estimated from the nearest true radiosounding to better emulate the real case. Radiosoundings at Schleswig (54:32N, 9:33O), Greifswald (54:06N, 13:24O), Emden-Königspolder (53:21N, 7:13O), Bergen (52:49N, 9:56O), Essen-Bredeney (51:24N, 6:58O), Fritzlar (51:08N, 9:17O), Oppin (51:33, 12:04O), Meiningen (50:34N, 10:23), Idar-Oberstein (49:42N, 7.20O), Stuttgart (48:50N, 9:12O), Kümmerbruck (49:26N, 11:54O) and Oberschleissheim (48:15N, 11:33O) from DWD are available for the days considered. At best radiosoundings at 0, 6, 12 and 18 UTC are available. The needed meteorological variables are taken from the nearest radiosounding in time and space.

4. Integral Radar Volume Descriptors

Using the threshold $\tau = 18\,\mathrm{dBZ}$ a verification of the basic equations (1) and (3) on the basis of the pseudo-radar data and the modelled rainfall showed that the unified theory provides only very crude rainfall estimates. For the first approach the rainfall amounts differ between $2.6 \cdot 10^8 \mathrm{m}^3$ and $1.53 \cdot 10^{14} \mathrm{m}^3$. Especially in case of small area-time integrals relative errors in excess of 500% are observed. The resulting relative error in V of 51 out of 100 rain events is larger than 100% if we apply the approach by keeping $S(\tau)$ constant. In 28 cases the relative error is smaller than 50%.

For the second approach the data set (events) at our disposal is much larger than in the first approach. In this case, a verification of equation (3) on the data showed that the error in $\langle R \rangle$ depends on the choice of the threshold parameter. For $F_0 = 0$ the error ranges between

an underestimation of max. 98% up to an overestimation of max. 1296%. In 15.3% of the testcases, the relative error was below 10% and in 30.2% of the testcases it was below 20%. If we slightly increase the threshold to $F_0 = 0.01$, the error remains in the same range for under– and overestimation. However, in 16.2% (31.6%) of the tests the error was below 10% (20%). For the largest threshold $F_0 = 0.05$ the maximal overestimation was significantly smaller (529%) than in the previous cases while the number of tests with errors below 10% and 20% could not be improved. Since the different choices of F_0 led to significantly different results in our verification, we distinguish these cases for the second approach what enables us to investige whether this effect can be eliminated by addition of further IRVDs or whether it is due to the model itself.

Altogether, we can conclude that the simple model by Doneaud et al. (1981) does not improve current quantitative rainfall estimations.

In our strategy to achieve enhanced space- and time-integrated rainfall estimates, we assume that the inclusion of further information on the spatial and temporal variability of the radar signal can be used in the future to guide or at least constrain static Z-R relations. We are guided by the assumption that useful information about the precipitation process can be extracted from the three-dimensional radar reflectivity structure, and that we will be able to obtain this information by the use of a few integral radar volume descriptors.

The definitions of considered IRVDs are listed below:

- Duration D: The length of the observation period of a raining system.
- Area-time integral ATI, Area $A(\tau)$, Area A_o, Fractional area $A(\tau)/A_o$ (see (2) and

(3)).

- Mean horizontal expected value *HMEAN* and mean horizontal standard deviation *HSTD*: In order to estimate the expected value and the standard deviation of the horizontally inclosed linear reflectivities at the ground, all accumulated values are interpreted as a realization of a Weibull distributed random variable to take into account the skewness and different shapes of the distribution (Rinne, 1997).

- Mean echo-top-height *METH*: The mean altitude above which the radar reflectivity is lower than 12dBZ (Rosenfeld, 1995a).

- Maximum vertical standard deviation *MVSTD*: The maximum standard deviation of the vertical reflectivity field at the center of reflectivity (analogue definition to centre of gravity) during the observation period.

- Temporally averaged vertical mean value *MVMEAN*: The temporal average of the mean values of the vertical reflectivity field at the center of reflectivity. The latter is defined similar to the center of gravity, i.e. the coordinates are weighted by the reflectivities.

- Mean brightband fraction *MBB*: The brightband fraction is the fraction of the echo area with maximum vertical reflectivities within $\pm 1\,\mathrm{km}$ of the $0^o\,C$ altitude. The calculation of the brightband fraction at different time steps of the observation period is very similar to the definition introduced by Rosenfeld et al. (1995a, 1995b). It is based on the $0^o\,C$ altitude estimated from the nearest radiosounding and on the vertical reflectivity field. Calculating the reflectivity field with a vertical resolution of

0.1 km at the center of reflectivity, the brightband fraction amounts to 1 for example, if all 21 values within ± 1 km from the $0^o\,C$ altitude are the maximum values below the echo-top-height. Considering a storm during its lifetime, the mean brightband fraction is calculated on the basis of all brightband fractions during the observation time steps.

- Mean effective efficiency ME_e: The definition of the effective efficiency E_e introduced by Rosenfeld et al. (1990) is based on the water vapor mixing ratios at the base (Q_b) and top (Q_t) of the cloud:

$$E_e = \frac{Q_b - Q_t}{Q_b}. \tag{5}$$

  Consequently, E_e describes the fraction of water vapor carried up through the cloud base which is potentially available for precipitation. Actual calculations use the saturation mixing ratios which are determined from the Magnus equation (Kraus, 2001) at 800m (Q_b) and at the echo-top-height (Q_t), respectively. The height of $800\,m$ represents a rough etimate for typical cloud-base conditions. The necessary meteorological variables like temperature or pressure at different heights are taken from the nearest radiosounding.

- Trends in *MBB* and trend-to-noise ratios: All descriptors mentioned above describe mean characteristics of the system or the considered raining area. However, a system undergoes changes in its characteristic during its lifetime. Major stages are the growing stage, the convective and the stratiform or dissipative stage. The trend in the brightband fraction should give an indication of the stage of evolution of the system during the observation; a positive (negative) trend in the brightband fraction indicates a system in the decaying (growing) stage. However, a variety of factors like the estimation

of the $0^o\,C$ level, splitting and merging of cells and, especially in the case of complex systems containing several small cells, the calculation of the brightband fraction at the center of reflectivity makes the signal noisy. Consequently, two different trend estimates are considered: the well-known least-squares estimator *TBB* of the linear trend in the observational brightband fraction and a robustified estimator *RTBB*. The latter is calculated by setting brightband fractions smaller than 0.1 equal to 0.1 and also by setting values larger than 0.9 equal to 0.9. Furthermore, the respective trend-to-noise ratios based on the least-squares estimator (*TNBB*) and the robustified estimator (*RTNBB*) are offered in order to represent the significance of the trend. The standard deviation of the brightband fraction *STDBB* is offered as self-contained descriptor, too.

- Orographic rainfall amplifier *ORO+* and *ORO±*: Roe (2005) assumed that the rate of condensation C of water vapor is very close to the temporal rate of change of the saturated moisture content. It provides an upper bound on the precipitation rate that can be achieved due to a to stable upslope ascent of saturated air, where at every level the vertical velocity equals the orographically forced lifting at the surface:

$$\begin{aligned} C &= -\int_{z_s}^{\infty} \vec{u} \cdot \nabla z_s \frac{d}{dz}[\rho q^{sat}] dz \\ &= \rho_0 q_0^{sat} \vec{u} \cdot \nabla z_s e^{-\frac{z_s}{H_m}} \end{aligned} \tag{6}$$

with the e-folding scale height for atmospheric moisture

$$H_m = -\frac{a}{b\Gamma},$$

where $a = 17.67$ and $b = 243.5^o\,C$, Γ is the temperature lapse rate, z_s the surface elevation, q^{sat} the saturation-specific humidity, ρ the air density, $\vec{u}$ the wind speed and

the subscript 0 denotes a variable's value at $z = 0$.

However, unlike Roe, we assume that saturation is not achieved until $800\,m$ height (cp. definition of the cloud base height in ME_e). Consequently, in our application ρ_0 and q_0 denote the air density and the saturation-specific humidity at height z, where

$$z \;=\; \max\{z_s\,,\,800m\}. \tag{7}$$

We estimate the vertical velocity $w = \vec{u} \cdot \nabla z_s$ using the difference in surface heights at the centers of reflectivity of a tracked cell in subsequent time steps and the temporal resolution ($600\,s$) of the radar data. Furthermore, we use the moist adiabatic lapse rate $\Gamma = 0.006^o C m^{-1}$, the temperature $T(z)$ and pressure $p(z)$ from the nearest radio sounding in order to estimate $q^{sat}(z)$ and the ideal gas law for estimation of the density $\rho(z)$.

The total condensation rate C_i is calculated for every time step during the observation period. The orographic rainfall amplifier *ORO+* summarizes all positive contributions C_i during the tracking period, while the descriptor *ORO±* summarizes all positive and negative contributions C_i during the tracking period. Consequently, the latter also takes into account negative values C_i due to a downslope descent.

- Mean wind shear *MSHEAR*: This descriptor includes the change in wind speed and direction with height in the atmosphere. Vertical wind shear lets the updraft separate from the downdraft, allowing the storm to survive longer and even become stronger. We define the mean wind shear *MSHEAR* as the average magnitude of wind vector difference in 850 and $500\,hPa$ during the observation period. Wind vectors are taken from the nearest radio sounding.

- Mean compactness *MCOM*: The compactness of a cell is the ratio of inclosed area to circumference. We suppose more intense convection with increasing compactness, i.e. stronger storms and convection in case of a continuous cell compared to a combination of several smaller cells. In order to avoid an increase of the descriptor with increasing size, we define the compactness of a system

$$COM = \frac{\sqrt{N_{in}}}{N_{out}}, \tag{8}$$

  where N_{in} is the number of inclosed pixels and N_{out} is the number of pixels on the edge of the cell. *MCOM* is defined as the average compactness during the observation period of the system.

The descriptors which include a characterization of the vertical structure of the reflectivity field are computed from the reflectivity field in 0.1 km resolution at the center of reflectivity of a cell at a time step. These IRVDs are the mean brightband fraction, the temporal trend in the brightband fraction, the mean effective efficiency, the mean echo-top-height, the maximum vertical standard deviation and the vertical mean value. Some descriptors provide information about the average state of the system during the observation period. In these cases, an averaging over the observation period is performed, e.g. the brightband fraction or the echo-top-height is determined for every time step of the observation period for the determination of the mean brightband fraction or the mean echo-top-height, respectively. Other descriptors contain cumulative information, e.g. the area A_o of the storm. In these cases, the inclosed area of the considered cell or any other parameter of each time step are accumulated to define the descriptors. Some descriptors, however, characterize the evolution of a system during its observation and thus can only be used for the instationary case (first

approach).

We now describe in detail the methods to enhance the estimation of the total rainfall of a storm during its lifetime and the instantaneous areawide rain rate, respectively.

5. Data regression

From the mathematical point of view, we make the assumption that a possibly nonlinear functional relation between the response variable y and the respective IRVD's exists, i.e. we assume that

$$y \;=\; f(x_1, \ldots, x_n). \tag{9}$$

In the first approach we have $y = V/ATI$, while for the second approach we define the response variable y as the quotient of $\langle R \rangle$ and $A(\tau)/A_o$. Each input variable $x_i,\ i = 1 \ldots n$, stands for one single IRVD. The function f has to be determined from discrete data points in such a manner that

(a) it fits well to the available data and

(b) gives good predictions for new data points.

In order to determine a function f fulfilling both requirements let f belong to a Hilbert space $\mathcal{H}$ and let $\mathcal{B} := \{\varphi_1, \varphi_2, \ldots\}$ be a basis of $\mathcal{H}$. Then, f can be expanded with real coefficients $c_1, c_2 \ldots$ in the infinite series

$$f(x_1, \ldots, x_n) \;=\; \sum_{i=1}^{\infty} c_i \, \varphi_i(x_1, \ldots, x_n). \tag{10}$$

For numerical computations, this expansion has to be discretized, i.e. the sum has to be truncated at a finite value ℓ. Since the resulting finite basis $\mathcal{B}_\ell$ is a subset of $\mathcal{B}$, it spans

a subspace $\mathcal{H}_\ell \subset \mathcal{H}$. The choice of the subspace $\mathcal{H}_\ell$ and its approximation properties for functions from $\mathcal{H}$ strongly affects the quality of the expected solutions.

Now, since the new IRVD's are collected in an n-dimensional vector $\mathbf{x} := (x_1, \ldots, x_n)^T$, where each component stands for an IRVD, the regressor has to be computed based on the given data points. Furthermore, we need a second data set to evaluate the quality of the computed regressor independently of the learning data. Therefore, we split the data at our disposal into a training- and a test-set of the form

$$\begin{aligned} \mathcal{P}_{train} &:= \{(y_1, \mathbf{x}_1), \ldots, (y_{P_1}, \mathbf{x}_{P_1})\} \quad \text{and} \\ \mathcal{P}_{test} &:= \{(\tilde{y}_1, \tilde{\mathbf{x}}_1), \ldots, (\tilde{y}_{P_2}, \tilde{\mathbf{x}}_{P_2})\}. \end{aligned} \tag{11}$$

The two sets are randomly sampled from the whole data set. They are of the same size and have no common elements. The overall error of the computed solution consists of two parts: The estimation error that depends on the choice of the training set $\mathcal{P}_{train}$ and the approximation error that depends on the approximation space $\mathcal{H}_{ell}$. From statistical learning theory, it is known that the estimation error can be reduced for fixed $\mathcal{H}_{ell}$ by an enlargement of the training data set. On the other hand, for a fixed size of the data set, the approximation error decreases when the space $\mathcal{H}_{ell}$ is enlarged, but the estimation error increases. This means that the overall error can only be reduced by an enlargement of both, the training set and the approximation space. Now, if the training set is small, like in the first approach, we have to restrict ourselfes to a relative small approximation space.

a. Multiple linear regression

In the first approach a well-known multiple linear regression is performed. In order to take into account possible non-linear relationships each of the 21 different descriptors is offered up to the power 5, resulting in 105 potential regressors. This corresponds to the choice of basis functions $\varphi_i(x_j) := x_j^i$, $j = 1, \ldots, 21$, $i = 1, \ldots, 5$, which results in the polynomial

$$\begin{aligned} f(x_1, \ldots, x_n) &= c_{1,1}\, x_1 + \ldots + c_{1,5}\, x_1^5 + \ldots \\ &\ldots + c_{21,1}\, x_{21} + \ldots + c_{21,5}\, x_{21}^5. \end{aligned} \tag{12}$$

A model selection criterion to deal with colinearities among the potential regressors and for developing parsimonious models is stepwise regression (Storch and Zwiers, 1999). This procedure combines forward selection and backward elimination steps. As forward selection progresses, descriptors selected early on may become redundant when related descriptors are selected during later steps. Therefore, in stepwise regression, backward elimination is performed after every forward selection step to remove unnecessary variables from the model, i.e. by setting the respective coefficients to $c_{j,i} = 0$. Forward selection and backward elimination steps are repeated until no further significant changes are made to the model.

For an evaluation of the rainfall estimates provided by the regression modell should be compared to those obtained from a fixed Z-R relation. However, in case of the pseudo-radar data used it would be an unfair game. As already mentioned in Section 3, reflectivities in the model are calculated using Rayleigh approximation and an exponential distribution (i.e. Marshall-Palmer for rain) for the precipitation particles. The spectral parameter Λ is replaced then by the predicted mass fraction. Consequently, a simple Z-R-relation would lead to an exact retrieval - it is a trivial solution for rain in a single-moment bulk scheme.

Alternatively, a leave-one-out cross-validation (LOOCV) is applied for an evaluation of the method. Thus, stepwise regression is performed 100 times on the basis of 99 of the rain events in order to calculate the error of the rainfall estimate of the remaining hundredth rain event.

For a larger approximation space, that also considers direct interactions of different variables, one would have to enhance the polynomial in (12) such that all mixed terms $x_i^a x_j^b,\ i,j = 1 \dots n$ and $a,b = 0 \dots p$ are present. This would enlarge the approximation space but result in $(p+1)^n$ terms. Therefore the complexity of the method would grow exponentially with the dimension n. Now, to handle the, also needed, large data sets and higher dimensional data an alternative regression method has to be employed. So, we use sparse grid regresssion for the second approach.

b. Sparse Grid regression

To find a function f that generalizes the relation between the response variable y and the IRVDs, we apply a sparse grid method (Garcke, 2004) for the large training and test sets from Section 5 resulting from the second approach. For large data sets there may exist approximation spaces $\mathcal{H}_\ell$ that are better adapted to the data than the space of polynomials. To achieve this, we apply hierarchical local basis functions, so called sparse grids (Bungartz and Griebel, 2004). Here, basis functions are constructed as tensor products of piecewise linear one-dimensional hierarchical basis functions with local support

$$\varphi_{\mathbf{i},\mathbf{k}}(\mathbf{x}) \ := \ \prod_{j=1}^{n} \varphi_{i_j,k_j}(x_j), \quad i_j \in \{1,2,\dots,J\}, \quad k_j \in \Lambda_{i_j} \tag{13}$$

and a fixed highest resolution level J. For a detailed description of the hierarchical basis and the definition of the resolution indices i_j and the location index sets Λ_{i_j} we refer to Yserentant (1992). This construction results in n-dimensional hierarchical basis functions with local support. Since in all coordinate directions, there exist 2^J hierarchical basis functions (on the interval) the overall number of basis functions is 2^{Jn}. Accordingly the complexity of the system increases exponentially with the dimensionality of the problem, a behaviour which is called the curse of dimensionality. To overcome this curse, the sparse grid method only takes into account basis functions with $i_1 + \ldots + i_n \leq J$. This reduces the number of degrees of freedom to $2^J J^{n-1}$. It can be shown that the same approximation rate is achieved as for the full grid if some regularity assumptions on $\mathcal{H}$ are made, namely $\mathcal{H}$ has to be the space H^1_{mix} of functions with bounded mixed derivatives. This space contains all functions f that have a finite norm

$$|| f ||_{H^1_{mix}([0,1]^n)} := \left(\int_{[0,1]^n} \left| \frac{\partial^n f(\mathbf{x})}{\partial x_1 \cdots \partial x_n} \right|^2 d\mathbf{x} \right)^{\frac{1}{2}}.$$

A common way to determine the function f from the given training set is to minimize the Tikhonov-regularized least-squares functional

$$E(f) := \frac{1}{P_1} \sum_{j=1}^{P_1} \Big(\sum_{i=1}^{\ell} c_i \, \varphi_i(\mathbf{x}_j) - y_j \Big)^2 + \lambda \left\| \sum_{i=1}^{\ell} c_i \, \varphi_i(\cdot) \right\|^2_{\mathcal{H}} \tag{14}$$

with respect to the real coefficients $c_1, \ldots, c_\ell$ using an appropriate norm $|| \cdot ||_{\mathcal{H}}$. The regularization factor $\lambda \in \mathbb{R}$ is used to balance the interpolation property enforced by the first term and the smoothness restrictions on f controlled by the norm. Therefore, (a) and (b) are reflected and balanced in one functional $E(f)$. Minimizing (14) with respect to the expansion coefficients leads to a sparse linear system of equations that can be solved by an iterative method such as the conjugate-gradient iteration.

6. Results

Now, we show numerical results for both approaches and the respective regression methods. The application of multiple linear regression to the first approach is presented in Section a while the sparse grid method is applied to the second approach in Section b.

a. First approach: total rainfall of a storm

The significance of a descriptor depends on the field of non-orthogonal descriptors out of which it is elected. In the following two different models are presented: For the first model we exlude the orographic rainfall amplifiers $ORO+$ and $ORO\pm$ and the wind shear *MSHEAR* from the pool of potential regressors while for the second model all descriptors listed in Section 4 are offered for detection. These are the only parameters, which are not directly related to or extracted from the structure of the radar returns. Thus they have a different quality and might also be more model resolution dependent than the others. For each model stepwise regression is applied 100 times to 99 values of V/ATI in order to explain remaining variability with a small set of the IRVD suite (cp. LOOCV described in Section a). Significant descriptors for the first and the second model and the frequency of their detection are listed in Table 2. So, the detection frequency of 100 for *HMEAN* means, that in all 100 regressions performances this descriptor is detected and makes a significant contribution. The descriptor $HMEAN^2$ instead is detected in 99 out of 100 cases. Accordingly, the detection frequency qualifies the sensitivity of a descriptors contribution to the regression model to small changes in the data set; a high detection frequency underlines the importance of the descriptor. Obviously, the additional potential descriptors lead to

considerable differences between both models.

The first model detects the same 7 descriptors in the majority of cases: the horizontal expected value in different powers *HMEAN*, $HMEAN^3$, $HMEAN^2$, the fractional area with reflectivities in excess of the threshold to the power of five $(A(\tau)/A_o)^5$, the horizontal standard deviation to the power of four $HSTD^4$, the mean brightband fraction to the power of three MBB^3 and the robustified estimate of the trend in the brightbandfraction *RTBB*. Noteworthy, that in most cases descriptors with a higher power are going along with very small coefficients. So, they are only important for rain events with high values of the respective descriptor.

On average the first model explains 98.93% of the remaining variance in V/ATI. The horizontal expected value *HMEAN* already explains about 95% of the variance. In Figure 2 the ratio V/ATI is drawn against this descriptor for the 100 rain events. Obviously, the superposition with the significant descriptors $HMEAN^3$ and $HMEAN^2$ achieves a degressive increase of V/ATI with increasing expected value.

Some explanatory notes are useful concerning the detected (robust) trend in the brightband fraction. As already mentioned, a positive trend mostly indicates a system in the decaying stage, and a negative trend indicates a system mostly in the growing stage. We found that a model equation based exclusively on descriptors reflecting the mean characteristics of the system tends to underestimate the total rainfall in case of a negative trend in the brightband fraction, i.e. in the growing stage, because maximum rainfall amounts are expected near the end of the growing stage. Analoguously, a model equation without information about the evolution the systems overestimates the total rainfall in case of a positive trend in the brightband fraction.

In the second model, the horizontal expected value remains the most important descriptor but the orographic rainfall amplifier *ORO+* is detected as an important information in all 100 cases, too. In the overwhelming majority of cases the horizontal expected value in different powers *HMEAN*, $HMEAN^3$, $HMEAN^2$, $HMEAN^4$, the orographic rainfall amplifier *ORO+*, the fractional area with reflectivities in excess of the threshold to the power of five $(A(\tau)/A_o)^5$ and the squared horizontal standard deviation $HSTD^2$ are aslo detected. In contrast to the first model, the frequency of the descriptor detection decreases less rapidly, and thus it is more difficult to fix a limit between the more and less important descriptors. On average, the second model explains 99.25% of the remaining variance in V/ATI.

Comparing the seven descriptors which have been most frequently detected by the two models, we find that the orographic rainfall amplifier takes over the place of the mean brightband fraction and its trend while the horizontal expected value, the fractional area with reflectivities larger τ and the horizontal standard deviation remain among the most relevant descriptors.

The resulting relative errors in the estimated accumulated rainfall based on the respective model equations including all significant detected regressors are shown in Figure 3. The maximum relative error in the first model amounts to 88.5%. This is, however, by far the largest error and it is associated with the smallest ratio $V/ATI = 0.88\,\mathrm{mm/h}$. In 74 (22) out of 100 rain events the relative error is smaller than 10% (2%). The maximum relative error in the second model amounts to 103.23%. In 79 (31) out of 100 rain events the relative error is smaller than 10% (2%). In summary, the second model keeps on reducing the smaller errors but gives also rise to single extreme high relative errors. However, reconsidering that systems of different scales with respect to the horizontal extent and rainfall amount (see

again Figure **??**) are traced over considerably different observation periods, both models show remarkably good results.

b. Second approach: instantaneous rain rate of many storms

The following stationary IRVDs from Section 4 are used to compute the quotient of instantaeous rain rate $\langle R \rangle$ and $A(\tau)/A_o$: *HSTD*, *METH*, *MBB*, ME_e and *MVSTD*. In addition to the last descriptor, we compute the horizontal average of the vertical mean of the reflecivities *HAVM*. To compute the respective descriptors we only include reflectivities that are above the threshold $\tau = 18\,\mathrm{dBZ}$. For our calculations, the coordinates $x_1, \ldots, x_6$ of the points in training and test set from Section 5 are these values.

Since we consider three different cases $F_0 \in \{0, 0.01, 0.05\}$, the sizes of the respective data sets differ. They are listed in Table 3. Then, the regressor f is computed by a minimization of the error functional (14) on the respective training set $\mathcal{P}_{train}$. To evaluate the result, the average of the relative error between the measured and the predicted value is computed on the test set $\mathcal{P}_{test}$. For each choice of the parameter a different models has been calculated. For $F_0 = 0$, we chose $J = 2$ and a regularization parameter $\lambda = 0.00001$, for $F_0 = 0.01$ we use the parameters $J = 3$ and $\lambda = 0.00001$ and in the last case $F_0 = 0.05$ we had $J = 2$ and $\lambda = 0.000001$. The results are depicted in Figure 4. Here, the test set is reordered with respect to the value of the errors and the regions below 10% and 20% have been marked light and dark shaded, respectively.

For the first case ($F_0 = 0$, $J = 2$, $\lambda = 0.00001$) the error ranges between an underestimation of $\langle R \rangle / (A(\tau)/A_0)$ by 222% and an overestimation by 1052%. For 67% of the events

the error is smaller than 20% and for 44% it is below 10%. The average relative error for the test set is 23.1%. In the second case ($F_0 = 0.01$, $J = 3$, $\lambda = 0.00001$) the predictions range from -143% to 614%. The average relative error is 12.0%, and 84.3% of the errors are below 20% while 58.3% are below 10%. In the last case ($F_0 = 0.05$, $J = 2$, $\lambda = 0.000001$) we achieved an average error of 10.3%. In 89.3% of the events the relative error was below 20% and in 66.2% it was below 10%. Here, we had a maximal undersetimation by 289% and a maximal overestimation by 250%.

For all models the resolution J is rather small what has a additional regularization effect on the model. This indicates that the learning data for the regression contained noise. Comparing these results with those from the verification in the second approach (see 4) we see that the consideration of the IRVD in the nonlinear model leads to significant improvements. Additionally, the dependence of the results from the choice of the threshold F_0 becomes clearly visible. Increasing its value leads to an improvement of the error. We conclude, that the second approach is not relieable if $A(\tau)/A_o \approx 0$.

To investigate the influence of each different IRVD on the error reduction we perform the same regression as before without the respective descriptor. This can be interpreted as a constant approximation in this coordinate direction. We restrict ourselves on the third case $F_0 = 0.05$, since this led to the best results in the previous calculations. The resulting relative errors can be found in Table 4.

The significance of the descriptors *HSTD*, *HAVM* is indicated by the fact that the test–errors become larger if they are left out of the regression process. Omitting the other descriptors in Table 4 only led to slightly increased errors, i.e. the dependence on these variables is weaker. Altogether, this leads to the conclusion that the high–dimensional

function $f(\mathbf{x})$, i.e. the quotient $\langle R \rangle / (A(\tau)/A_o)$ depending on the IRVDs, has a small gradient.

7. Conclusions and Outlook

Analyses based on rainfall and pseudo-radar data simulated by the weather forecast model COSMO-DE were performed in order to test and extend the unified theory by Atlas et al. (1990) for the estimation of the total rainfall produced by an individual storm (first approach) and the estimation of areawide instantaneous rainfall (second approach). Subsequent verification of the accuracy showed that further exploitation of the spatial and temporal variability of the radar signal in terms of IRVD can significantly enhance the rainfall estimates. Doneaud et al. (1981) first employed the area-time integral ATI, Altas et al. (1990) added the fractional area $A(\tau)/A_o$ to the framework of the unified theory and Rosenfeld (1990) already achieved better results accounting also for the effective efficiency E_e. We also used the definition of the brighband fraction introduced by Rosenfeld et al. (1995a, 1995b) for the classification of rain regimes, but we additionally extended the pool of potential descriptors with descriptors not yet utilized in radar meteorology. The horizontal expected value, the horizontal standard deviation, the orographic rainfall amplifier and the trend in the brightband fraction as an indicator for the stage of evolution of the system are the most promising new descriptors presented. It is worth mentioning that the accuracy of some descriptors strongly depends on the availiability of different meteorological variables (see again Section 3) which are necessary for their estimation. In this study, the respective information was taken from 12 different radiosounding stations with up to 4 measurements, respectively.

In order to enhance the estimation of the accumulated rainfall of an individual storm, in the first approach stepwise regression is applied as model selection criterion in order to achieve a parsimonious multiple regression model. Two different models have been considered; only the second model takes information about the wind profile and the surface elevation into account. Leave-one-out cross-validation shows that in 74 (79) out of 100 rain events the relative error is smaller than 10% in the first (second) model.

For the second approach, the computation of the stationary IRVDs is simpler and the same data lead to much larger training and test sets. Here we applied a high–dimensional sparse grid regression method with Thikonov regularization. We distinguished three different cases to compute the data samples. For each case, different models with different discretization levels and regularization parameters have been considered. For the third case, we could achieve in 66.2% percent of the testcases an error that was below 10%.

Evidently, an evaluation of the models against real radar data and observational precipitation is the next important step. The effects of additional noise caused by radar-based errors (e.g. clutter, attenuation) and a yet unsufficient data base for observed precipitation need to addressed. We plan to use radar data to interpolate between the high-resolution rain-gauge stations in order to construct a resolution-wise adequate while inaccurate data set for surface rainfall. Here we have to deal with the problem, that the radar data will be used both for g̈round truthänd for estimation (see again Hagen et al., 2003). This impact, however, is likely small because the information taken from the radar as information source will be the IRVDs, which have no direct relation to the information obtained from the radar to construct the ground truth. Alternatively, we can use the model equations obtained from our current results and statistically compare the results of their application to real radar

data against surface rain gauges. This approach should at least be able to decide whether the precipitation dynamics and microphysics in the model is comparable to reality, leading to a new method for model validation.

8. Acknowledgments

We gratefully acknowledge the funding of the German Research Foundation (DFG) under grants Si606/8-2 and Gr1144/15-2 within the context of the Project Cluster AQUARadar (http://www.meteo.uni-bonn.de/projekte/aquaradar-wiki). We also thank DWD for providing the COSMO-DE model and Felix Ament and Annika Schomburg for making the model runs.

REFERENCES

Atlas, D., Rosenfeld, D. and Short, D. A. 1990. The Estimation of Convective Rainfall by Area Integrals. 1. The Theoretical and Empirical Basis. *J. Geophys. Res.* **95**, 2153–2160

Bungartz, H. J. and Griebel, M 2004. Sparse Grids. *Acta Numerica* **13**,1–123

Doms, G. and Schättler, U. 2002. A description of the nonhydrostatic regional model LM. Part 1: Dynamics and Numerics. *Deutscher Wetterdienst (DWD), Offenbach.* 1–134

Doms, G., Förstner, J., Heise, E., Herzog, H.-J., Raschendorfer, M., Schrodin, R., Reinhardt,

T. and Vogel, G. 2005. A description of the Nonhydrostatic Regional Model LM. Part 2: Physical Parameterization (only draft version). *Deutscher Wetterdienst (DWD), Offenbach (http://www.cosmo-model.org)*. 1–118

Doneaud, A. A., Smith, P. L., Dennis, A. S. and Sengupta, S. 1981. A simple method for Estimating Convective Rain Volume Over an Area. *Water Resour. Res.* **17**, 1676–1682

Fabry, F., Austin, G. L. and Tees, D. 1992. The accuracy of rainfall estimates by radar as a function of range. *Q. J. R. Meteorol. Soc.* **118**, 435–453

Garcke, J. 2004. *Maschinelles Lernen durch Funktionsrekonstruktion mit verallgemeinerten dünnen Gittern*. Doktorarbeit, Institut für Numerische Simulation Universität Bonn (in german).

Garcke, J., Griebel, M. and Thess, M. 2001. Data mining with sparse grids. *Computing* **67:3**, 225–253

Hagen, M., Frei, C. and Schär, C. 2003. Temporal disaggregation of rain-gauge analyses using radar. *Presentation at the Int. Conf. Alpine Meteorol. and MAP-meeting*, Brig, Switzerland.

Kessler, E. 1969. On the distribution and continuity of water substance in atmospheric circulation. *Meteor. Monogr.* **10**, No.32, 1–84

Krajewski, W. F. and Smith, J. A. 2002. Radar hydrology: rainfall estimation. *Ad. Water Res.* **25**, 1387–1394

Kraus, H. 2001. *Die Atmosphäre der Erde*, Springer Verlag, Berlin, Heidelberg, New York.

Auth13] Lopez, R. E., Thomas, J., Blanchard, O. and Holle, R. L. 1983. Estimation of rainfall over an extended region using only measurements of the area covered by radar echoes, paper presented at the 21st Conference on Radar Meteorology, Am. Meteorol. Soc., Edmonton, Alberta, Canada, Sept. 19-23, 1983.

Marshall, J. S., Palmer, W. McK. 1948. The distribution of raindrops with size. *J. Meteor.* **5**, 165–166

Marshall, J. S., Hitschfeld, W. and Gunn, K. L. S. 1955. Advances in radar weather. *Adv. in Geophys.* **2**, 1–56

Rinne, H. 1997. *Taschenbuch der Statistik*, 2., überarb. und erw. Aufl., Verlag Harri Deutsch, Thun und Frankfurt am Main, 1–650.

Roe, G. H. 2005. Orographic Precipitation. *Annu. Rev. Earth Planet. Sci.* **33**, 645–671

Rosenfeld, D., Atlas, D. and Short, D. A. 1990. The Estimation of Convective Rainfall by Area Integrals. 2. The Height-Area Rainfall Threshold (HART) Method. *J. Geophys. Res.* **95**, 2161–2176

Rosenfeld, D., and Amitai, E. 1995. Classification of Rain Regimes by the Three-Dimensional Properties of Reflectivity Fields. *J. Appl. Meteor.* **34**, 198–211

Rosenfeld, D., Amitai, E. and Wolff, D. B. 1995b. Improved Accuracy of Radar WPMM Estimation Rainfall upon Application of Objective Classification Criteria. *J. Appl. Meteor.* **34**, 212–223

Ryzhkov, A. V., Giangrande, S. E. and Schuur, T. J. 2005. Rainfall Estimation with a Polarimetric Prototype of WSR-88D. *J. Appl. Meteor.* **44**, 502–515

Sauvageot, H. 1992. *Radar Meteorology*, Artech House Publishers, Norwood, 384pp.

Simon, J. L. 2004. *Tracking of Radar-Detected Precipitation-Centroids using Scale-Space Methods for Automatic Focussing*. Diplomarbeit, Mathematisch-Naturwissenschaftliche Fakultät der Rheinischen Friedrich-Wilhelm-Universität zu Bonn.

Storch, H. v. and Zwiers, F. W. 1999. *Statistical Analysis in Climate Research*, Cambridge University Press, Cambridge, 484pp..

Yserentant, H. 1992. Hierarchical bases. In: *Proc. ICIAM'91*, (eds. R. E. O'Malley), SIAM, Philadelphia, 281–290.

List of Figures

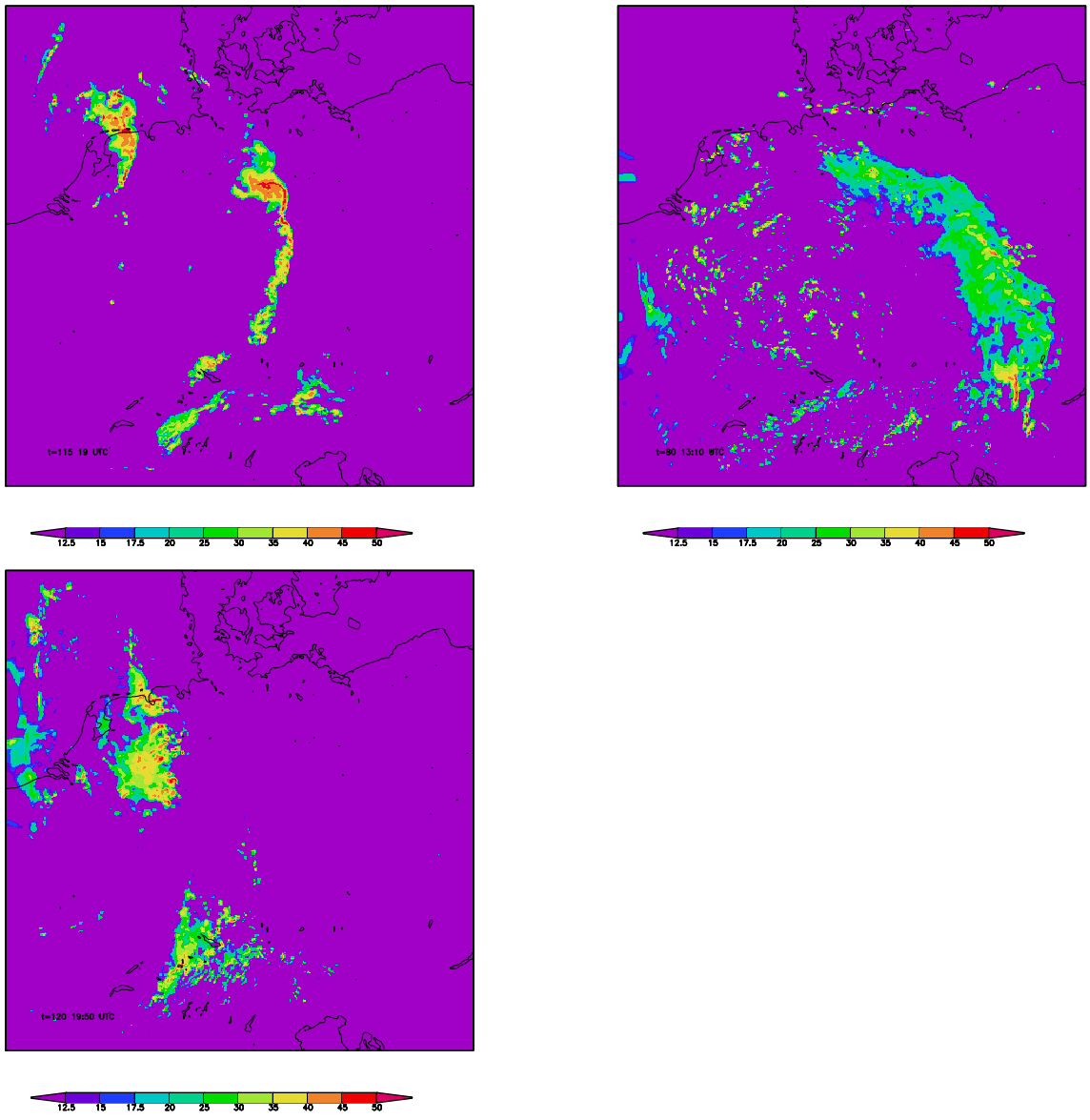

FIG. *1. One snapshot showing the pseudo-reflectivities (COSMO-DE) in dBZ in the bottom layer from July 17, 2004 (top), July 8, 2005 (middle) and August 19, 2005 (bottom), respectively.*

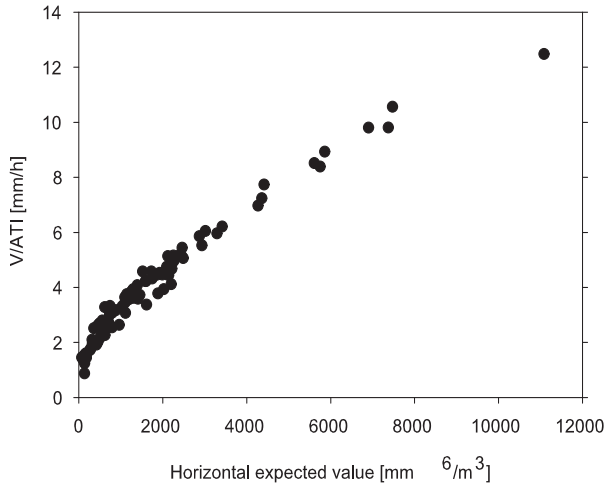

FIG. *2. Horizontal expected value of inclosed linear reflectivites HMEAN versus V/ATI.*

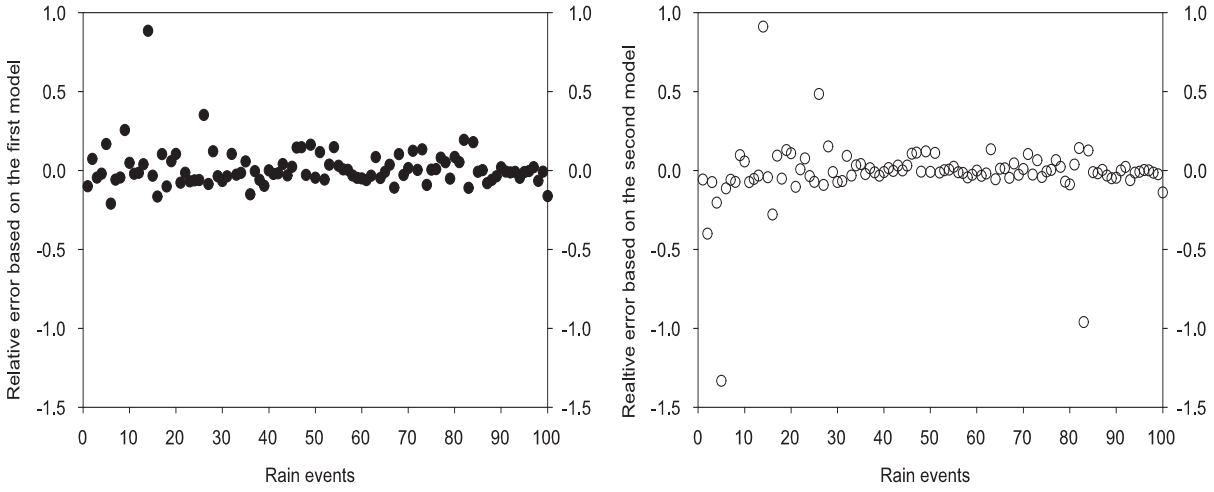

FIG. *3. Relative error in estimated precipitation sums applying the first (top) and the second model (bottom) in the first approach, respectively.*

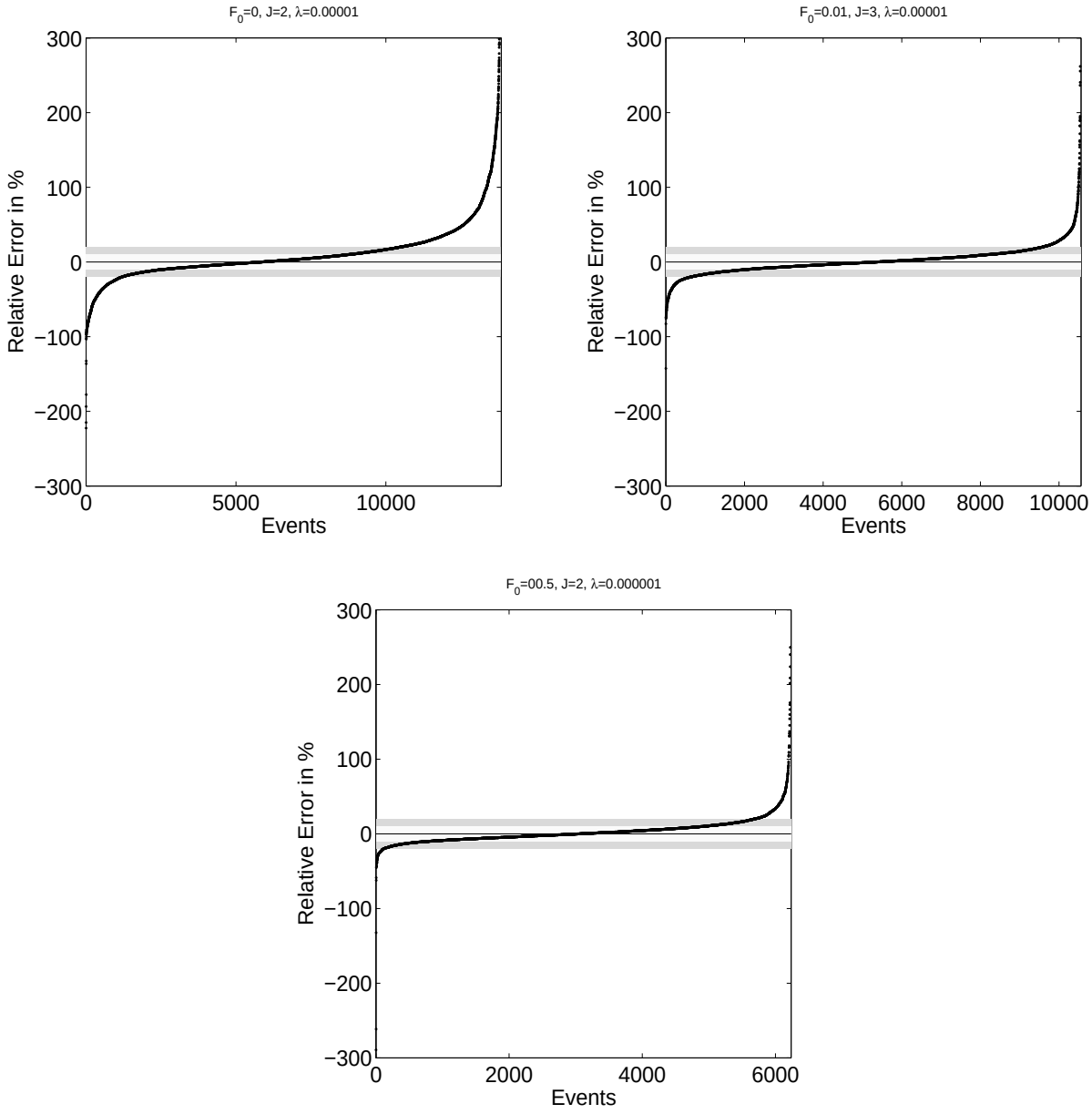

FIG. *4. The relative errors of all elements from the respective test-set for each case.* $F_0 = 0$ *is shown in the top left figure,* $F_0 = 0.01$ *in the top right and* $F_0 = 0.05$ *in the bottom figure. For each result the test-set has been reordered with respect to the error for clarity. The shaded regions mark the elements with a 10% (light) and 20% (dark) error. We only show errors in the range of* $\pm 300\%$.

List of Tables

TABLE *1. Distribution of 100 traced raining systems over the days considered and a priori applied Gaussian smoothing (σ in number of rid-cells in one direction) of the reflectivity field.*

Date	Gauss kernel's σ	Number of rain events
July 17, 2004	6	26
	14	6
July 8, 2005	6	15
	10	20
	14	5
August 19, 2005	6	16
	10	12

TABLE *2. Significant detected descriptors and the frequency of their detection with and without taking into account the orographic rainfall amplifier and the wind shear, denoted as the first and the second model, respectively.*

Significant descriptor in the first model	Frequency
$HMEAN$	100
$HMEAN^3$	100
$HMEAN^2$	99
$(A(\tau)/A_o)^5$	99
$HSTD^4$	98
MBB^3	97
$RTBB$	87
ME_e	17
$(A(\tau)/A_o)$	9
TBB^3	8
$TNBB^3$	7
$HMEAN^4$	2
TBB^5	1

Significant descriptor in the second model	Frequency
$HMEAN$	100
$HMEAN^3$	100
$HMEAN^2$	100
$ORO+$	100
$(A(\tau)/A_o)^5$	99
$HMEAN^4$	91
$HSTD^2$	90
D	65
$ORO+^2$	65
$MSHEAR^3$	58
$ORO\pm^4$	43
$MSHEAR^2$	16
$ORO\pm^3$	16

TABLE 3. *Sizes of training– and test set for the different values of* F_0.

F_0	0	0.01	0.05
size of $\mathcal{P}_{train}$	13848	10560	6236
size of $\mathcal{P}_{test}$	13848	10559	6235

TABLE *4. The following errors were achieved for the case* $F_0 = 0.05$ *in the second approach if the descriptor in the first column was not included in the calculation.*

Omitted parameter	Average error in %
none	10.3
HSTD	18.0
ME_e	10.6
MBB	10.8
METH	10.8
HAVM	11.0
MVSTD	10.7